Wide-Speed Operation of Direct Torque-Controlled Interior Permanent-Magnet Synchronous Motors

Adina Muntean, M.M. Radulescu
Small Electric Motors and Electric Traction (SEMET) Group, Technical University of Cluj-Napoca
P.O. Box 345, RO-400110 Cluj-Napoca 1, Romania, e-mail: mircea.radulescu@mae.utcluj.ro

A. Miraoui
Laboratory of Electronics, Electrotechnics and Systems (L2ES), University of Technology
of Belfort-Montbéliard, rue Thierry-Mieg, F-90010 Belfort, France, e-mail: abdellatif.miraoui@utbm.fr

***Abstract* - In this paper, an integrated design and direct torque control (DTC) of inverter-fed interior permanent-magnet synchronous motors (IPMSMs) for wide-speed operation with high torque capability is presented. The double-layer IPM rotor design is accounted for IPMSMs requiring a wide torque-speed envelope. A novel approach for the generation of the reference stator flux-linkage magnitude is developed in the proposed IPMSM DTC scheme to insure extended torque-speed envelope with maximum-torque-per-stator-current operation range below the base speed as well as constant-power flux-weakening and maximum-torque-per-stator-flux operation regions above the base speed. Simulation results to show the effectiveness of the proposed DTC scheme are provided and discussed.**

I. INTRODUCTION

Due to their many positive features, including high torque-to-inertia and power-to-weight ratios, fast dynamics, compact design and low maintenance, inverter-fed interior permanent-magnet synchronous motors (IPMSMs) are viable contenders for industrial drives with high torque capability over a wide speed range. Indeed, PMs being completely embedded inside the steel rotor core, a mechanically robust construction of IPMSMs allowing wide speed-torque envelope is primarily obtained. Secondly, the rotor-buried PMs, covered by steel pole-pieces, significantly change the magnetic circuit of the motor, since, on the one hand, the PM cavities create flux barriers within the rotor, thus reducing the permeance in a flux direction that crosses these cavities, and, on the other hand, high-permeance paths are created for the flux across the steel rotor poles and also in space-quadrature to the rotor-PM flux; this establishes the rotor magnetic saliency. Hence, it is a hybrid torque production mechanism in IPMSMs, because in addition to the magnet (or field-alignment) torque due to the interaction of rotor-PM flux and the armature (stator) mmf, there is also a reluctance torque component due to rotor magnetic saliency. Thirdly, IPMSM having a small effective airgap, the armature reaction is quite important, and can be conveniently used for airgap flux weakening in order to extend the motor torque capability towards high speeds.

Several current vector control schemes were earlier proposed for wide-speed range control of IPMSMs, the motor torque being indirectly controlled via subordinated stator current loops [1-3]. All these control schemes are based on steady-state motor characteristics, whereas the IPMSM dynamic behaviour is implicitly solved by the current controller.

Recently, the direct torque control (DTC) has been proposed for high-performance wide-speed operation of IPMSMs [4-7]. In principle, the IPMSM DTC involves the direct and independent control of the stator flux-linkages and the electromagnetic torque by selecting proper voltage switching vectors of the voltage-source inverter (VSI) supplying the motor. This selection is made to restrict the differences between the references of stator flux-linkage magnitude and electromagnetic torque and their actual (estimated) values. The advantages of the IPMSM DTC over conventional current control schemes include the elimination of current controller, coordinate transformation and PWM signal generator, the lesser dependence on motor parameters as well as the fast torque response in steady-state and transient operating conditions.

In this paper, an integrated design and DTC of VSI-fed IPMSMs for wide-speed operation with high torque capability is presented. Hence, the paper is organized as follows. In Section II, the double-layer IPM-rotor design is adopted for IPMSMs requiring a wide torque-speed envelope. In Section III, an IPMSM DTC scheme incorporating both the optimised constant-torque and flux-weakening controllers for wide-speed range operation is developed. Simulation results to validate the proposed IPMSM DTC scheme are presented and discussed in Section IV. Conclusions are drawn in Section V.

II. IPMSM DESIGN FOR WIDE-SPEED OPERATION

The stator of the considered VSI-fed IPMSM is a typical AC design accommodating a three-phase distributed winding in slots to produce the synchronously-rotating, quasi-sinusoidal armature-mmf wave. Conversely, the IPMSM rotor can be designed in different configurations. However, only two of them with radially-magnetized buried-type IPMs have been accounted as being advantageous for wide-speed operation [8-10]. The high-energy rotor-PMs usually consist of sintered-NdFeB blocks inserted after magnetization into the rotor cavities.

Fig. 1 shows the cross-sectional configurations of both IPMSMs in conjunction with their rated-load magnetic flux distribution obtained from finite element analysis. The first IPMSM rotor topology has only one (single-layer) PM per rotor-pole, whereas in the second one, each rotor-PM is splitted up in two layers with iron separation in the radial direction of the rotor core.

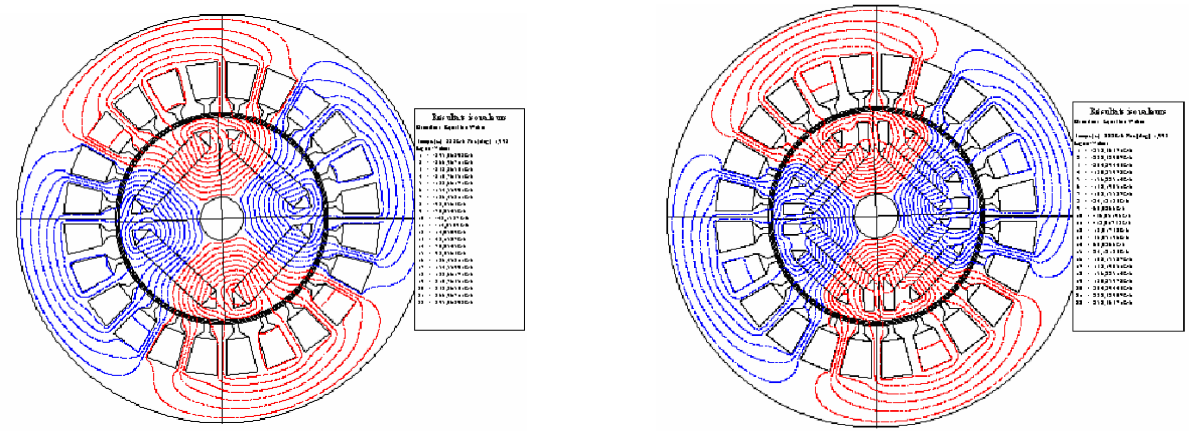

(a) (b)

Fig. 1. IPMSM cross-sectional design and magnetic flux distribution under rated-load condition for (*a*) single- and (*b*) double-layer IPM rotor topology, respectively.

The well-known coordinate system (*d*,*q*) bounded to the rotor (i.e. rotating at synchronous speed ω_r) is defined hereafter with the *d*-axis aligned with the stator PM flux-linkage vector $\underline{\psi}_{s0} = \underline{\psi}_{PM}$ and the orthogonal *q*-axis aligned with the back-emf vector $\omega_r \underline{\psi}_{PM}$ (Fig. 2). By noticing that the (total) stator flux-linkage vector can be splitted into the flux linkage (with the stator winding) due to the excitation rotor-PMs, $\underline{\psi}_{PM}$, and the armature-reaction flux, which entails the self-inductances L_{sd} and L_{sq} ($L_{sd} < L_{sq}$) of the stator winding along the *d*- and *q*-axis, respectively, the IPMSM electromagnetic torque may be expressed as [5, 6]

$$m_e = (3p/2)\,|\underline{\psi}_s|\,(|\underline{\psi}_{PM}| - \xi\,|\underline{\psi}_s|\cos\delta)\sin\delta / L_{sq}\,(1-\xi), \quad (1)$$

where $\xi = (L_{sq} - L_{sd}) / L_{sq}$ defines the magnetic saliency ratio, and δ represents the angle between flux-linkage vectors $\underline{\psi}_s$ and $\underline{\psi}_{PM}$ (Fig.2); δ is constant for steady-state operation, hence both $\underline{\psi}_s$ and $\underline{\psi}_{PM}$ vectors rotate at synchronous speed ω_r; in transient operation, δ varies, hence $\underline{\psi}_s$ and $\underline{\psi}_{PM}$ rotate at different speeds, $\omega_s \neq \omega_r$.

It can be identified in Eq.(1) the first IPMSM torque component, as the magnet (or field-alignment) torque and the second one, as the reluctance torque due to rotor magnetic saliency. From Eq.(1), it also results that, for a certain stator flux-linkage vector modulus $|\underline{\psi}_s|$, the IPMSM rotor design achieving high torque capability over a wide-speed operation range requires increased values of the rotor-PM linkage flux magnitude $|\underline{\psi}_{PM}|$ and of the stator self-inductance difference $L_{sq} - L_{sd}$.

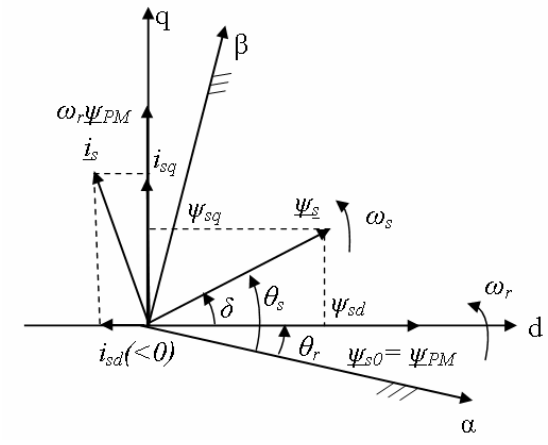

Fig. 2. Different coordinate systems for vector representation of IPMSM quantities.

A comparison between the two IPMSM rotor designs of Fig.1, for constant rotor-PM volume and for identical magnetic properties, rotor outer diameter, airgap and stator specifications, has been made in order to select the most suitable structure for high-torque wide-speed operation. As result of this comparison based on finite-element magnetic field analysis of both IPMSMs, the double-layer IPM rotor design has been adopted for motor prototype by the following reasons.

(i) The *d*-axis stator self-inductance L_{sd} is low and roughly the same for both single- and double-layer PM-rotor configurations.

(ii) The *q*-axis stator self-inductance L_{sq} and, correspondingly, the inductance difference $L_{sq} - L_{sd}$ for the double-layer IPM rotor is up to 20% greater than for the single-layer IPM rotor, mainly due to the additional *q*-axis flux path provided between the two rotor-PM layers.

(iii) The *q*-axis stator self-inductance L_{sq} for the rotor topology with only one PM per pole decreases greatly with the stator-current rising, because of the magnetic saturation, whereas for the double-layer PM-rotor topology this effect is less significant.

(iv) The stator flux-linkage due to the double-layer of rotor PMs is about 10% greater than in the case of single-layer IPM rotor.

(v) The electromagnetic torque developed up to the rated rotor speed by the double-layer IPMSM is about 10% increased in comparison with that produced by a single-layer IPMSM, for the same armature mmf. However, the torque performances using flux-weakening at high speeds for both IPMSMs are quite similar.

III. DTC OF VSI-FED IPMSM FOR WIDE-SPEED OPERATION

In the DTC scheme for VSI-fed IPMSM, the inner torque controller is based on the expression of the electromagnetic

torque given by Eq.(1). Hence, torque is controlled by regulating (through inverter voltages) the amplitude $|\underline{\psi}_s|$ and the angle δ of the stator flux-linkage vector.
The d- and q-axis stator flux linkages are

$$\psi_{sd} = L_{sd}\, i_{sd} + |\underline{\psi}_{PM}| \quad (2)$$
$$\psi_{sq} = L_{sq}\, i_{sq}\,. \quad (3)$$

From Eqs. (2) and (3), the stator flux-linkage vector modulus can be expressed as

$$|\underline{\psi}_s| = (\psi_{sd}^2 + \psi_{sq}^2)^{1/2} = [(L_{sd}\, i_{sd} + |\underline{\psi}_{PM}|)^2 + (L_{sq}\, i_{sq})^2]^{1/2}. \quad (4)$$

By differentiating Eq.(1) with respect to time, for constant stator flux-linkage magnitude, one obtains

$$dm_e/dt = (3p/2)|\underline{\psi}_s|(|\underline{\psi}_{PM}|\cos\delta - \xi\,|\underline{\psi}_s|\cos 2\delta)(d\delta/dt)\,/L_{sq}(1-\xi). \quad (5)$$

Eq.(5) emphasizes that the electromagnetic torque can be dynamically controlled by means of controlling the rate of change of the angle δ.
There are upper limits of variation for both control quantities, $|\underline{\psi}_s|$ and δ, to achieve stable IPMSM DTC. Firstly, since according to Eq.(1), m_e=0 for δ=0, the condition for positive slope $dm_e/d\delta$ around $\delta = 0$ leads to

$$|\underline{\psi}_s| < |\underline{\psi}_{PM}| / \xi. \quad (6)$$

Secondly, by differentiating Eq.(1) with respect to δ and equating it to zero, the maximum allowable angle δ_{lim} can be found as

$$\delta_{lim} = \cos^{-1}\{|\underline{\psi}_{PM}|/ 4\xi\,|\underline{\psi}_s| - [(|\underline{\psi}_{PM}| / 4\xi\,|\underline{\psi}_s|)^2 + 1/2]^{1/2}\}, \quad (7)$$

that is
$$\delta \le \delta_{lim}. \quad (8)$$

The block diagram of the proposed DTC scheme for wide-speed operation with high torque capability of a VSI-fed IPMSM is shown in Fig.3. The three-phase stator variables are transformed to the α,β-axes variables of the (α,β) stationary coordinate system shown in Fig. 2.

The α,β stator currents, obtained from current sensors, and the stator voltages $u_{s\alpha}$ and $u_{s\beta}$, calculated from the measured DC-link voltage, are then used for stator flux-linkage vector and electromagnetic torque estimation. Some methods of compensation for the effect of stator resistance variation and for the DC offset in the measurements, particularly at low speed, have been recently reported [11-12]. The initial angular position of the stator flux–linkage vector $\underline{\psi}_s$ may be obtained from a low-resolution encoder. Subsequently, this encoder is not needed under the DTC scheme.
Electromagnetic torque and stator flux-linkage magnitude errors, generated by comparison between estimated and reference values, are inputs to the respective flux and torque hysteresis regulators. The discretized outputs of these regulators are inputs to the optimum voltage switching selection table. It is used to properly choose the VSI-fed voltage vectors to regulate the stator flux and torque within their error bands.
In the IPMSM DTC scheme of Fig.3, the reference electromagnetic torque, $m_{e,ref}$, is obtained as the output of the rotor-speed controller from the outer loop, and is limited at a certain value, which guarantees the stator current not to exceed its maximum admissible value.
In its turn, the reference value of the stator flux-linkage vector modulus, $|\underline{\psi}_{s,ref}|$, is generated in the proposed IPMSM DTC scheme as a function of the electromagnetic torque reference, i.e. $|\underline{\psi}_{s,ref}|(m_{e,ref})$, by maximizing the IPMSM torque over the wide-speed operation range in the presence of current and voltage constraints.
The stator current limit, $I_{s,lim}$, is an IPMSM thermal rating or a VSI maximum available current. The stator voltage limit, $U_{s,lim}$, is the VSI maximum available output voltage, depending on the DC-link voltage. Hence, the current and voltage constraints establish the following operating limits for the VSI-fed IPMSM:

$$|\underline{i}_s| = (i_{sd}^2 + i_{sq}^2)^{1/2} \le I_{s,lim}\,, \quad (9)$$
$$|\underline{u}_s| = (u_{sd}^2 + u_{sq}^2)^{1/2} \le U_{s,lim}\,. \quad (10)$$

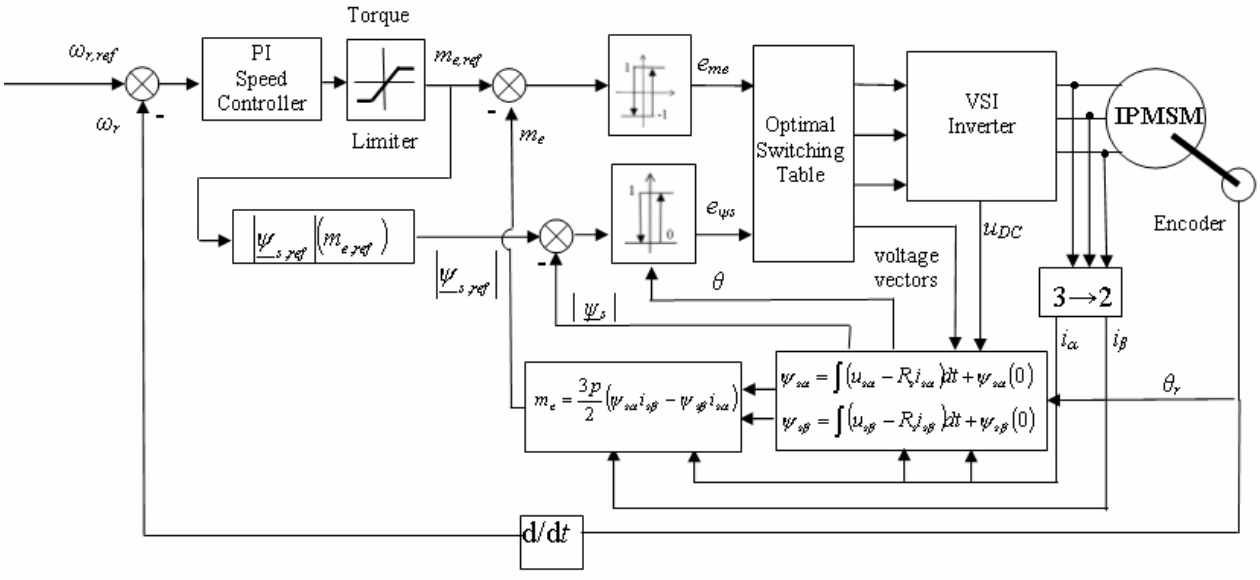

Fig. 3. Block diagram of the VSI-fed IPMSM DTC scheme for wide-speed operation.

In the speed operation range I from standstill up to the base rotor speed ω_{rb} , current constraint of Eq.(9) is dominant, preventing the IPMSM overheating, whereas voltage constraint of Eq.(10) can be met, since the back-emf is rather low. Thus, the required function $|\underline{\psi}_{s,refI}|(m_{e,refI})$ for the reference value of the stator flux-linkage magnitude in the speed range I can be obtained by ensuring the IPMSM constant-torque operation in which the maximum torque-to-stator current ratio is achieved at the stator-current limit $I_{s,lim}$, i.e. the motor is accelerated by the maximum available torque below the base speed; it results

$$(i_{sd,I}^2 + i_{sq,I}^2)^{1/2} = I_{s,lim}, \quad (11)$$

$$m_{e,maxI} = (3p/4)\,|\underline{\psi}_{PM}|\, i_{sq,I}\{1 + [1 + (2\xi L_{sq}\, i_{sq,I} / |\underline{\psi}_{PM}|)^2]^{1/2}\}. \quad (12)$$

For the currents $i_{sd,I}$ and $i_{sq,I}$, Eq.(5) can be written as

$$|\underline{\psi}_{s,refI}| = [(L_{sd}\, i_{sd,I} + |\underline{\psi}_{PM}|)^2 + (L_{sq}\, i_{sq,I})^2]^{1/2}. \quad (13)$$

Considering in Eq.(12) $m_{e,maxI} = m_{e,refI}$, solving Eqs.(11) and (12) for the currents $i_{sd,I}$ and $i_{sq,I}$, and then substituting in Eq.(13), one obtains the function $|\underline{\psi}_{s,refI}|(m_{e,refI})$ requested in the IPMSM DTC scheme over the speed range I, i.e. from standstill up to the base rotor speed ω_{rb}. If one defines ω_{rb} as the highest speed for the constant-torque operation mode with the maximum torque subject to the stator-current limit, and, at the same time, as the lowest speed for which the stator-voltage limit is reached, ω_{rb} can be readily deduced from the steady-state IPMSM stator voltage equations in the (d,q) coordinate system (neglecting the stator-resistance voltage drop):

$$u_{sd} = -\omega_r L_{sq}\, i_{sq}, \quad (14)$$

$$u_{sq} = \omega_r L_{sd}\, i_{sd} + \omega_r |\underline{\psi}_{PM}|; \quad (15)$$

one obtains from Eqs.(13)-(15)

$$\omega_{rb} = U_{s,lim} / [(L_{sd}\, i_{sd,I} + |\underline{\psi}_{PM}|)^2 + (L_{sq}\, i_{sq,I})^2]^{1/2}. \quad (16)$$

The IPMSM speed operation range II, just above the base rotor speed, is a flux-weakening constant-power region. The highest attainable IPMSM torque subject to both stator current and voltage limits of Eqs.(9) and (10) yields

$$m_{e,maxII} = (3p/2)\,[|\underline{\psi}_{PM}|\, i_{sq,II} - (L_{sq} - L_{sd})\, i_{sd,II}\, i_{sq,II}], \quad (17)$$

where

$$(i_{sd,II}^2 + i_{sq,II}^2)^{1/2} = I_{s,lim}, \quad (18)$$

$$i_{sd,II} = \big(|\underline{\psi}_{PM}|\, L_{sd} - \{(|\underline{\psi}_{PM}|\, L_{sd})^2 + (L_{sq}^2 - L_{sd}^2) \times [|\underline{\psi}_{PM}|^2 + (L_{sq}\, I_{s,lim})^2 - (U_{s,lim}/\omega_r)^2]\}^{1/2}\big)/(L_{sq}^2 - L_{sd}^2). \quad (19)$$

Rewriting Eq.(13) for $i_{sd,II}$ and $i_{sq,II}$, accounting in Eq.(17) $m_{e,maxII} = m_{e,refII}$, and eliminating the currents $i_{sd,II}$ and $i_{sq,II}$ between Eqs.(13) and (17)-(19), one obtains the required function $|\underline{\psi}_{s,refII}|(m_{e,refII})$ for the IPMSM DTC scheme over the flux-weakening constant-power speed range II.

Since for the considered IPMSM drive $|\underline{\psi}_{PM}| / L_{sd} < I_{s,lim}$, there is a high-speed flux-weakening region III, where IPMSM constant-power operation is no more achievable. However, the torque capability can be insured by the maximum torque-to-stator flux ratio subject to the stator voltage limit alone. The rotor speed, at which IPMSM constant-power operation ceases, is termed as base power speed, ω_{rbp}, and can be simply determined by

$$\omega_{rbp} = U_{s,lim} / (L_{sd}\, I_{s,lim} - |\underline{\psi}_{PM}|). \quad (20)$$

Beyond ω_{rbp}, IPMSM flux-weakening operation is still available up to theoretically infinite speed.

The IPMSM maximum available torque, $m_{e,maxIII}$, as previously defined for the high-speed flux-weakening operation range III, is determined by introducing the upper-limit angle δ_{lim} of Eq.(8) into Eq.(1) expressing the IPMSM torque, thus leading to

$$m_{e,maxIII} = (3p/2)\,|\underline{\psi}_s|\,\big(|\underline{\psi}_{PM}| - \xi\,|\underline{\psi}_s|\,\{|\underline{\psi}_{PM}|/4\xi\,|\underline{\psi}_s| - [(|\underline{\psi}_{PM}|/4\xi\,|\underline{\psi}_s|)^2 + 1/2]^{1/2}\}\big) \times\big(1 - \{|\underline{\psi}_{PM}|/4\xi\,|\underline{\psi}_s| - [(|\underline{\psi}_{PM}|/4\xi\,|\underline{\psi}_s|)^2 + 1/2]^{1/2}\}^2\big) / L_{sq}(1-\xi). \quad (21)$$

Eq.(21) with $m_{e,maxIII} = m_{e,refIII}$, yields the required function $|\underline{\psi}_{s,refIII}|(m_{e,refIII})$ for the IPMSM DTC scheme over the high-speed flux-weakening operation range III.

For the three IPMSM operation modes that have been previously identified over the wide speed range (below and above the base speed) the specific reference relationships $|\underline{\psi}_{s,ref}|(m_{e,ref})$ can be computed off-line, and subsequently incorporated into the IPMSM DTC scheme as a simple look-up table.

IV. SIMULATION RESULTS

Extensive dynamic simulations using Matlab / Simulink software are carried out on a prototype IPMSM having the specifications given in Table 1 in order to validate and assess the performance of the proposed VSI-fed IPMSM DTC scheme over wide-speed operation range.

Fig. 4 shows the simulated dynamic responses of DTC IPMSM speed, torque and stator flux-linkage with respect to a step change in speed reference from 0 to 4000 rpm under no-load condition and subject to current and voltage constraints. It is seen from Fig. 4, that a smooth transition between the constant-torque and flux-weakening speed operation regions occurs when the rotor speed exceeds the base speed. With the proposed DTC scheme, IPMSM is accelerated by the maximum available torque in both constant-torque and flux-weakening operation modes over the wide speed range in the presence of current and voltage constraints. Fig. 4,*d* displays the dynamic locus of the stator flux-linkage vector, which is almost a circle in both constant-torque and flux-weakening wide-speed operation ranges.

Table 1. Specifications of prototype IPMSM

Number of pole-pairs, p	3	
Stator phase resistance, R_s	0.895	Ω
PM flux-linkage magnitude, $\lvert\underline{\psi}_{PM}\rvert$	0.2979	Wb
d-axis stator self-inductance, L_{sd}	12.16	mH
q-axis stator self-inductance, L_{sq}	21.3	mH
Stator current limit, $I_{s,lim}$	6.75	A
Stator voltage limit, $U_{s,lim}$	400	V
Base rotor speed, ω_{rb}	2500	rpm

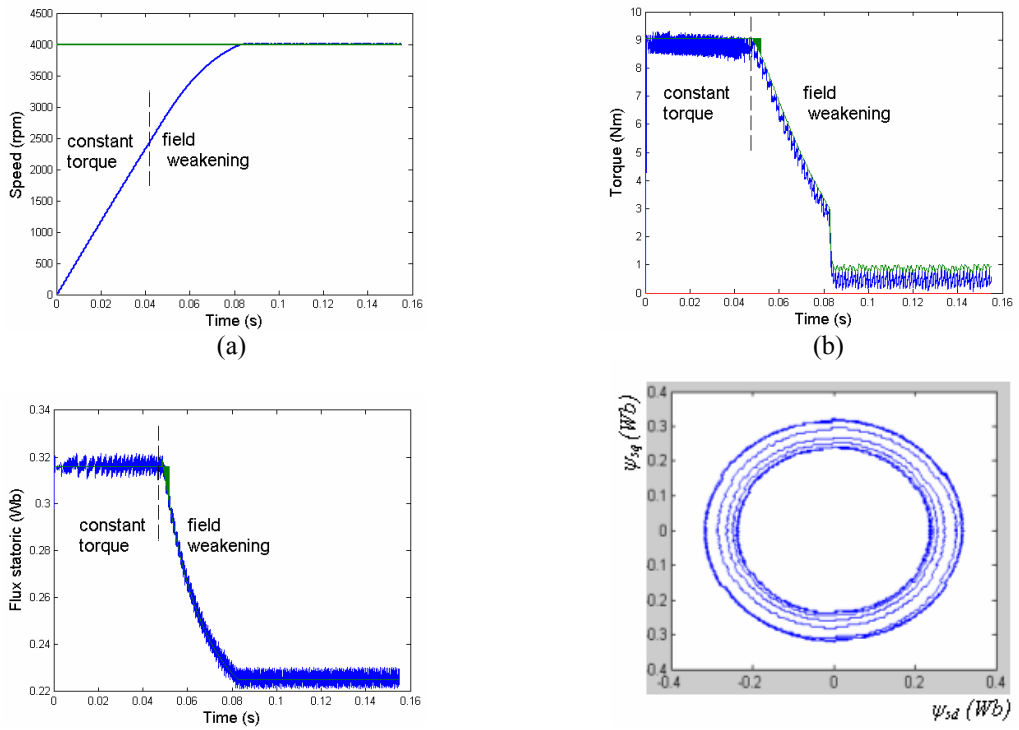

Fig. 4. Dynamic simulation results for prototype IPMSM DTC over constant-torque and flux-weakening wide-speed operation ranges: (*a*) rotor-speed response; (*b*) torque response; (c) response of the stator flux-linkage magnitude; (d) locus of the stator flux-linkage vector.

V. CONCLUSIONS

An integrated approach to the proper design and DTC of VSI-fed IPMSMs requiring wide speed-torque envelope has been proposed.

The relationship between the reference electromagnetic torque and stator flux-linkage has been derived to be used in IPMSM DTC insuring maximum-torque-per-stator-current operation below the base speed as well as constant-power flux-weakening and maximum-torque-per-stator-flux operations above the base speed.

The simulated dynamic response in step speed command has confirmed the effectiveness of the proposed IPMSM DTC scheme over wide-speed operation range.

REFERENCES

[1] Morimoto, S., Sanada, M. and Takeda, Y. "Wide-speed operation of interior permanent magnet synchronous motors with high-performance current regulator". *IEEE Trans. Ind. Applic.*, vol. 30, no. 4, pp. 920-926, 1994.

[2] Kim, J.-M. and Sul, S.-K., "Speed control of interior permanent magnet synchronous motor drive for the flux weakening operation". *IEEE Trans. Ind. Applic.*, vol. 33, no.1, pp. 43-48, 1997.

[3] Uddin, M.N., Radwan, T.S. and Rahman, M.A., "Performance of interior permanent magnet motor drive over wide speed range". *IEEE Trans. Energy Convers.*, vol. 17, no. 1, pp. 79-84, 2002.

[4] Rahman, M.F., Zhong, L. and Lim, K.W., "A direct torque-controlled interior permanent magnet synchronous motor drive incorporating field weakening". *IEEE Trans. Ind. Applic.*, vol.34, no. 6, pp. 1246-1253, 1998.

[5] Vas, P., "*Sensorless vector and direct torque control*". Oxford University Press, Oxford, UK, 1998, ch. 3, pp. 223-237.

[6] Luukko, J., "*Direct torque control of permanent magnet synchronous machines – Analysis and implementation*". Ph.D. Dissertation, Lappeenranta University of Technology, Finland, 2000, 172 pp.

[7] Qinghua, L., Khambadkone, A.M., Tripathi, A. and Jabbar, M.A., "Torque control of IPMSM drives using direct flux control for wide speed operation". *Proc. IEEE Int. Conf. Electr. Mach. Drives Conf.* (*IEMDC 2003*), vol. 1, pp. 188-193, 1-4 June 2003, Madison, Wisconsin, USA.

[8] Honda, Y., Higaki, T., Morimoto, S. and Takeda, Y., "Rotor design optimization of a multi-layer interior permanent-magnet synchronous motor". *IEE Proc. – Electr. Power Applic.*, vol. 145, no. 2, pp. 119-124, 1998.

[9] Qinghua, L., Jabbar, M.A. and Khambadkone, A.M., "Design optimization of a wide-speed permanent magnet synchronous motor". *Proc. IEE Int. Conf. Power Electron. Mach. Drives* (*PEMD 2002*), pp. 404-408, 16-18 April 2002 , Bath, UK.

[10] Rahman, F. and Dutta, R., "A new rotor of IPM machine suitable for wide speed range". *Rec. 29th Ann. Conf. IEEE Ind. Electron. Soc. (IECON 2003)*, CD-ROM, 2-6 November 2003, Roanoke, Virginia, USA.

[11] Luukko, J., Niemelä, M. and Pyrhönen, J., "Estimation of the flux linkage in a direct-torque-controlled drive". *IEEE Trans. Ind. Electron.,* vol. 50, no. 2, pp. 283-287, 2003.

[12] Tang, L., Rahman, F. and Haque, M.E., "Low speed performance improvement of a direct torque controlled interior permanent magnet synchronous machine drive". *Rec. 19th IEEE Ann. Appl. Power Electron. Conf. (APEC 2004)*, pp. 558-564, 22-26 February 2004, Anaheim, California, USA.